Direct Mixed-Quantum/Classical Computations of $k(T)$. An Analysis of the Use of Different Coordinate Systems

ESTEBAN CLAVERO, JULIANA PALMA

Centro de Estudios e Investigaciones, Universidad Nacional de Quilmes, Sáenz Peña 352, B1876BXD, Bernal, Argentina

Received 10 March 2010; accepted 2 April 2010
Published online 31 August 2010 in Wiley Online Library (wileyonlinelibrary.com).
DOI 10.1002/qua.22775

ABSTRACT: We have obtained three mixed-quantum/classical schemes to directly calculate thermal rate constants through the evaluation of flux-flux correlation function. These schemes are appropriate to treat three-atom reactions, but could be easily extended to larger systems. One of the schemes uses normal mode coordinates, defined at the transition state. The others use hyperspherical coordinates. The proposed algorithms were applied to the $H+H_2 \rightarrow H_2+H$ reaction, and their accuracy was tested by comparison with full-quantum results. In this article, we present the derivation of the three mixed-quantum/classical schemes, describe the details of their implementation, and discuss the quality of their results. Int J Quantum Chem 111: 1773–1783, 2011

Key words: reaction dynamics; thermal rate constants; mixed-quantum/classical; flux-flux correlation function

1. Introduction

In a recent article [1] we applied a mixed-quantum/classical (Q/C) version of the flux–flux correlation function method to directly calculate thermal rate constants for a model system. The model, previously introduced by McRae et al. [2] consisted of an Eckart barrier resembling the collinear $H+H_2 \rightarrow H_2+H$ reaction, bilinearly coupled to a harmonic oscillator. The frequency of the oscillator and the coupling constant were varied over a wide range of values, following the prescriptions given in Ref. [2]. It was found that the approximated rate constants closely match the exact ones, except when the system forms long-lived complexes. This finding suggests that mixed-Q/C computations of the reactive flux could constitute a relatively simple and efficient way to calculate $k(T)$ of gas-phase reactions that proceed without forming such complexes. Among the advantages of the approach, we mention its conceptual simplicity, its relatively low computational cost, and its ability to take into account

Correspondence to: J. Palma; e-mail: juliana@unq.edu.ar
Contract grant sponsors: CONICET and the Universidad Nacional de Quilmes.

tunnelling and recrossings without needing *ad hoc* corrections. However, a significant difference exists between applying the Q/C-approach to a model instead of an actual reactive system. In the model, it is usually known in advance which are the quantum and the classical degrees of freedom. Moreover, the coupling between them is explicitly given as a part of the model. On the contrary, in the study of any realistic system, one has to decide which coordinates to use and how to allocate them into the classical and quantum subsystems. These choices implicitly determine the strength of the coupling between the parts and, therefore, have a large influence on the accuracy of the results.

The description of many mixed-Q/C treatments of gas-phase reactions can be found in the literature [3–19], and important lessons about the strengths and weaknesses of the approach can be learnt from those works. However, to the best of our knowledge, none of the previous studies used the Q/C approach to estimate $k(T)$ through the computation of the flux–flux correlation function. Instead, the treatments were based on a time-dependent implementation of the reactive scattering theory. In such applications, the trajectories are initiated with the reactants molecules far away from each other and are propagated until the products leave the strong interaction region. Because of this, the propagation times are significantly larger than those needed to evaluate the flux-flux correlation function. Since the error of mixed-Q/C trajectories increases by increasing the propagation time, mixed-Q/C evaluations of the flux-flux correlation function could provide a more accurate way of determining $k(T)$ than that provided by the reactive scattering formalism. Besides, during computations of the flux-flux correlation function, the trajectories sample a relatively small region of the potential energy surface (PES) around the transition state (TS). For this limited region, it is not so difficult to find coordinates that produce a fairly good separation between the subsystems. This is not the case of reactive scattering computations because the trajectories must sample large parts of the PES. On the other hand, mixed-Q/C direct computations of $k(T)$ have been described for Hamiltonian models corresponding to condensed-phase reactions [20, 21]. However, such processes are qualitatively different from reactions in gas phase because of the different role played by the "bath" coordinates.

The degrees of freedom required for the description of a general polyatomic reaction can be classified according to the type of motion they describe. In turn, this classification can be used as a guide at the time of defining a mixed-Q/C scheme suitable for the reaction of interest. So, for example, some degrees of freedom are related to the internal vibrations of the nonreactive fragments. In most cases, it seems reasonable to assume that an approximate treatment of such modes will not have a large impact on the quality of the final results. On the contrary, the coordinate or coordinates describing the bonds being broken and formed clearly require an accurate treatment. A third coordinate set is related to the degrees of freedom describing the rotational motion of reactants and products. These modes become bending vibrations at the TS that, in some cases, can reach relatively high frequencies. For this reason, it is difficult to predict the effect of treating them classically. Finally, some degrees of freedom are required to account for the rotation of the system as a whole.

We have developed mixed-Q/C schemes to compute the flux-flux correlation function of three-atom reactions and applied them to the simplest reactive system, $H+H_2 \rightarrow H_2+H$. However, we should note that the schemes presented here could easily be extended to treat polyatomic systems. We have analyzed, in particular, the quality of the mixed-Q/C approach when the bending vibration of the TS is treated classically. Two different coordinate sets were tested: hyperspherical coordinates and TS normal modes. We have considered that the atoms move on a two-dimensional space, i.e., they move on the $\{x, y\}$ plane. This allowed us to perform full-quantum (full-QM) computations easily and quickly, even for $J \neq 0$. The strategy is justified by a recent study of Wang [16], which indicates that the accuracy of Q/C computations, performed on reduced-dimensionality (RD) models, can be used to infer the quality of the approach when applied to the exact Hamiltonian from which the RD models were extracted.

The effective Hamiltonians used in the mixed-Q/C calculations were derived from the ones used in the full-QM calculations, following the prescriptions given by Gerber et al. [22] In some cases, additional approximations were introduced to obtain simpler propagation schemes. We take care that all the parameters, such as masses and conversion constants, were exactly the same in both full-QM and mixed-Q/C computations. Therefore, the differences between them can only be attributed to the limitations of the Q/C algorithms being tested, given a truthful assessment of their ability to estimate $k(T)$.

In the next section, we present the mixed-Q/C schemes and describe the methodology used to carry

out both full-QM and mixed-Q/C computations. Then, in Section 3, we present the results. In particular, we compare the predictions of the different Q/C schemes, between each other and with the full-QM computations. On the basis of these comparisons, we discuss the pros and cons of the Q/C algorithms. Finally, in Section 4, we outline the conclusions of this work.

2. Methodology

2.1. FULL-QM AND MIXED-QC COMPUTATIONS OF THE REACTIVE FLUX

Miller et al. [23] demonstrated that the rate constants for a gas-phase reaction can be accurately calculated from

$$Q_r(T)k(T) = \int_0^\infty C_{\rm ff}(t)dt, \tag{1}$$

where $Q_r(T)$ is the reactants partition function per unit volume and $C_{\rm ff}(t)$ is the flux–flux correlation function,

$$C_{\rm ff}(t) = {\rm Tr}\big[\hat{F}(\beta)e^{i\hat{H}t/\hbar}\hat{F}e^{-i\hat{H}t/\hbar}\big]. \tag{2}$$

Here $\hat{F} = [\hat{H}, h]$ is the flux operator, h is the Heaviside step function, $\beta = (kT)^{-1}$, and $\hat{F}(\beta)$ is the Boltzmannized flux operator

$$\hat{F}(\beta) = e^{-\beta\hat{H}/2}\hat{F}e^{-\beta\hat{H}/2}. \tag{3}$$

By introducing the spectral decomposition of $\hat{F}(\beta)$ into Eq. (2), a numerically convenient expression is obtained to evaluate $C_{\rm ff}(t)$ [20],

$$C_{\rm ff}(t) = \sum_{j=1}^{N_f} f_j \langle u_j(t)|\hat{F}|u_j(t)\rangle. \tag{4}$$

In this expression, f_j and $|u_j\rangle$ are the eigenvalues and eigenfunctions of $\hat{F}(\beta)$, respectively, $N_{\rm f}$ is the number of such eigenfunctions with non-negligible eigenvalues, and the $|u_{\rm j}(t)\rangle$ is the time-evolved eigenfunction of $\hat{F}(\beta)$,

$$|u_{\rm j}(t)\rangle = e^{-i\hat{H}t/\hbar}|u_{\rm j}\rangle. \tag{5}$$

To perform the mixed-Q/C computations, the Hamiltonian is written as [1, 20]

$$H = \hat{H}_s + H_b^{\#} + V_{\rm coup}(\mathbf{s}, \mathbf{r}). \tag{6}$$

In this equation, $\hat{H}_s$ is the quantum Hamiltonian of the "system," which only groups a selected set of coordinates, **s**, and their conjugated momenta. Ideally, **s** includes all the modes directly involved in the reactive event. On the other hand, $H_{\rm b}^{\#}$ is the classical Hamiltonian of the "bath," which depends on the rest of the coordinates, **r**, and their conjugated momenta. The superscript in $H_{\rm b}^{\#}$ indicates that the classical coordinates are defined by setting the quantum subsystem at the TS. Finally, the last term of Eq. (6) is a coupling potential that renders the full Hamiltonian nonseparable.

The mixed-Q/C estimation to the flux–flux correlation function, $C_{\rm ff}^{\rm QC}$, is evaluated as [20],

$$C_{\rm ff}^{\rm QC} = Q_{\rm b}^{\#}\frac{1}{N_{\rm traj}}\sum_{n=1}^{N_{\rm traj}}\sum_{j=1}^{N_f} f_{\rm s,j}\langle u_{s,j}^n(t)|\hat{F}_{\rm s}|u_{\rm s,j}^n(t)\rangle_{\rm s}. \tag{7}$$

In this expression $N_{\rm traj}$ is the number of trajectories, $Q_{\rm b}^{\#}$ is the partition function for the classical degrees of freedom at the transition state, $\hat{F}_{\rm s} = [\hat{H}_{\rm s}, h]$ is the flux operator for the quantum subsystem, whereas $f_{\rm s,j}$ and $|u_{\rm s,j}\rangle$ are the eigenvalues and eigenfunctions of $\hat{F}_{\rm s}(\beta)$, respectively. The trajectories of Eq. (7) are initiated by selecting the classical coordinates and momenta at random from their classical distribution probabilities, whereas the quantum subsystem is set at a given eigenstate of $\hat{F}_{\rm s}(\beta)$. Then, the trajectories are integrated using a mixed-Q/C propagation scheme. In such a scheme, the evolution of the $|u_{\rm s,j}\rangle$ is obtained from the application of the time-dependent Schrödinger equation corresponding to the effective Hamiltonian,

$$\hat{H}_{\rm s}^{\rm eff} = \hat{H}_{\rm s} + V_{\rm coup}(\mathbf{s}, \mathbf{r}(t)). \tag{8}$$

The evolution of the classical variables is calculated from the canonical equations with the effective classical Hamiltonian,

$$H_b^{\rm eff} = H_b^{\#} + \langle u_{s,j}(t)|V_{\rm coup}|u_{s,j}(t)\rangle_s. \tag{9}$$

The symbol $\langle\ldots\rangle_s$ in the last equation denotes integration over the whole range of the quantum variables.

2.2. MIXED-QUANTUM/CLASSICAL SCHEMES

The Hamiltonian of a reactive system can be written in several equivalent ways by using different coordinates. Clearly, the application of any of these Hamiltonians in full-QM computations renders exactly the same results, assuming that enough

computational resources are available so as to get converged values in every case. This does not hold true for mixed-Q/C computations, because the application of different coordinates allows for a variety of ways of partitioning the whole system into the quantum and classical subsystems [20]. In the following, we derive the effective Hamiltonians to be used in mixed-Q/C computations of the reactive flux for three-atom reactions. We will use both transition-state normal modes and hyperspherical coordinates to evaluate which of the two options is the most convenient.

2.2.1. Transition State Normal Modes

Computations using normal-mode coordinates were only performed for zero total angular momentum. The corresponding Hamiltonian is

$$\hat{H}^{\mathrm{NM}}_{\mathrm{J}=0} = \frac{1}{2}\left(\hat{p}_1^2 + \hat{p}_2^2 + \hat{p}_3^2\right) + V(q_1, q_2, q_3). \tag{10}$$

In this equation, q_1, q_2, and q_3 are the mass-weighted normal-mode coordinates at the transition state, whereas $\hat{p}_1$, $\hat{p}_2$, and $\hat{p}_3$ are their conjugate momenta. Coordinate q_1 stands for the asymmetric stretching vibration, it has an imaginary frequency and corresponds to the reaction coordinate at the TS. On the other hand, coordinate q_2 stands for the symmetric stretching vibration, which modulates the distance between the donor and the acceptor atoms. Finally, coordinate q_3 corresponds to a bending vibration that correlates with the rotational motion of the H_2 molecule, at the asymptotic regions of the surface.

After deciding the coordinate system to be used, two important decisions have to be made to define a mixed-Q/C scheme. First, one has to allocate the coordinates into the quantum and classical subsystems. In this case, we considered that the quantum subsystem was composed by the stretching coordinates q_1 and q_2, whereas q_3 was set at the classical subsystem. Second, one has to decide the potentials appearing in the quantum and classical Hamiltonians. This decision is crucial, because it implicitly defines the coupling potential. The smaller the coupling in the region sampled by the eigenfunctions of $\hat{F}_{\mathrm{s}}(\beta)$, the better the approximation. With this idea in mind, we defined the potential for the quantum system as

$$V_{\mathrm{s}}(q_1, q_2) = V(q_1, q_2, q_3 = 0),$$

while the potential of the classical bath was as follows,

$$V_b(q_3) = V(q_1 = 0, q_2 = 0, q_3).$$

Accordingly, the coupling potential was given as,

$$V_{\mathrm{coup}}(q_1, q_2, q_3) = V(q_1, q_2, q_3) - \left(V_s(q_1, q_2) + V_{\mathrm{b}}(q_3)\right). \tag{11}$$

We found that this definition produced much better results than the one obtained by using harmonic potentials for each subsystem. This is because the harmonic approximation is good only within a very small region around the TS, whereas the eigenfunctions of $\hat{F}(\beta)$ spread over a significantly wider region. Finally, following procedure Gerber et al. [22], we obtained the effective quantum and classical Hamiltonians to be used in mixed-Q/C computations,

$$\begin{aligned}\hat{H}^{\mathrm{eff}}_{\mathrm{s}} &= -\frac{\hbar^2}{2}\left(\frac{\partial^2}{\partial q_1^2} + \frac{\partial^2}{\partial q_2^2}\right) + V_s(q_1, q_2) \\ &\quad + V_{\mathrm{coup}}(q_1, q_2, q_3(t)), \\ H^{\mathrm{eff}}_{\mathrm{b}} &= \frac{p_3^2}{2} + V_{\mathrm{b}}(q_3) + \langle V_{\mathrm{coup}}(q_1, q_2, q_3)\rangle_{q_1, q_2}.\end{aligned}$$

2.2.2. Hyperspherical Coordinates

Using hyperspherical coordinates, the Hamiltonian for the planar H+H_2 →H_2+H reaction can be written as,

$$\hat{H} = \hat{H}^{\mathrm{HS}}_{\mathrm{J}=0} + \hat{K}_{\mathrm{rot}}, \tag{12}$$

with,

$$\begin{aligned}\hat{H}^{\mathrm{HS}}_{\mathrm{J}=0} &= -\frac{\hbar^2}{2\mu}\left(\frac{\partial^2}{\partial\rho^2} + \frac{1}{\rho^2}\frac{\partial^2}{\partial\delta^2}\right) - \frac{\hbar^2}{2I_\alpha(\rho,\delta)}\frac{\partial^2}{\partial\alpha^2} \\ &\quad - \frac{\hbar^2}{8}\left(\frac{1}{I_\alpha(\rho,\delta)} + \frac{1}{I_\beta(\rho)}\right) + V(\rho, \delta, \alpha).\end{aligned} \tag{13}$$

In this expression, ρ and δ are the hyperradius and hyperangle, respectively, defined in terms of the length of the Jacobi vectors **r** and **R** (see Fig. 1),

$$\begin{aligned}\rho &= (r^2 + R^2)^{1/2}, \\ \delta &= \arctan(r/R),\end{aligned}$$

while α is the angle between these vectors. The reduced mass μ is given by $\mu = m_1 m_2 m_3/(m_1 + m_2 + m_3)$ where m_i is the mass of the i-atom. The moment of inertia $I_\alpha(\rho, \delta)$, associated with the hindered rotation of vector **R** around the center of mass of H_2, is given by

$$I_\alpha(\rho, \delta) = \mu\rho^2 \sin^2\delta \cos^2\delta, \tag{14}$$

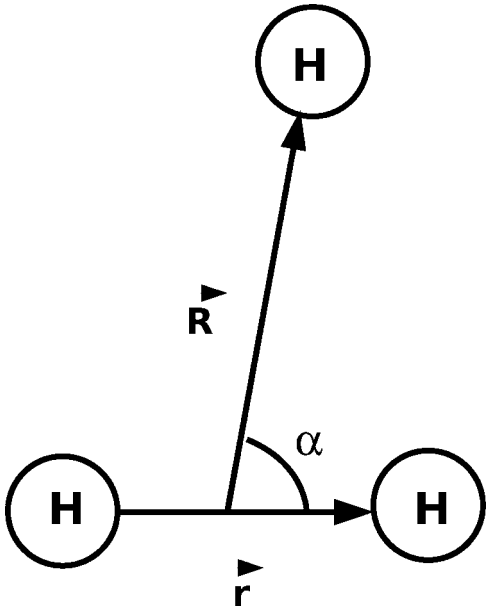

FIGURE 1. Jacobi vectors and bending angle used to derive the Hamiltonian of Eq. (12).

while the moment of inertia $I_\beta(\rho)$, associated with the rotation of the whole system, takes the form

$$I_\beta(\rho) = \mu\rho^2. \tag{15}$$

Finally, the operator $\hat{K}_{\text{rot}}$ that accounts for the kinetic energy of the rotation is

$$\hat{K}_{\text{rot}} = \frac{\hat{J}^2}{2I_\beta(\rho)}. \tag{16}$$

As the total angular momentum is a good quantum number, the operator $\hat{J}$ can be replaced by its eigenvalues. Then, the term corresponding to $\hat{K}_{\text{rot}}$ can be added to $V(\rho,\delta,\alpha)$ to define an effective potential, $V^J(\rho,\delta,\alpha)$, for each total angular momentum. Moreover, we also included in $V^J(\rho,\delta,\alpha)$ the terms $-\hbar^2/8I_\beta(\rho)$ and $-\hbar^2/8I_\alpha(\rho,\delta)$ that appear in Eq. (13) because of the scaling of the wave function. This scaling only involves the variables ρ and δ, and renders the following volume element,

$$d\tau = d\rho d\delta d\alpha. \tag{17}$$

In the same spirit of the treatment given in normal modes, we defined the mixed-quantum/classical scheme by allocating the hyperspherical coordinates, which describe the stretching vibrations at the TS, into the quantum subsystem. The angle α, which accounts for the bending vibration, was put at the classical subsystem. The potential for the quantum Hamiltonian was defined as

$$V_{\text{s}}^J(\rho,\delta) = V^J(\rho,\delta,\alpha=\alpha^\#),$$

whereas for the classical Hamiltonian we set

$$V_{\text{b}}^J(\alpha) = V^J(\rho=\rho^\#,\delta=\delta^\#,\alpha).$$

With these definitions, the coupling potential is given by

$$V_{\text{coup}}(\rho,\delta,\alpha) = V^J(\rho,\delta,\alpha) - \left(V_{\text{s}}^J(\rho,\delta) + V_b^J(\alpha)\right).$$

The application of the procedure of Gerber et al. to the Hamiltonian of Eq. (13), with the allocation of coordinates already described, produces equations of motion which look slightly different than the standard ones. This is because the kinetic energy term in α also depends on ρ and δ. Accordingly, Eq. (13) cannot be written in the form required by Eq. (6). We show in the Appendix the derivation of the effective Hamiltonians obtained by applying the procedure of Gerber et al. to the full-QM Hamiltonian of Eq. (13). However, in the rest of the article, we present and discuss two simpler approximations in which the equations of motion maintain the standard form. This simplification is achieved by replacing the factor $1/I_\alpha(\rho,\delta)$ appearing in Eq. (13) by a constant value. In the "mean field" approximation (HSMF), we average $1/I_\alpha(\rho,\delta)$ over the wave function corresponding to the initial quantum state. This value is then used throughout the whole propagation. In the second and even simpler approximation (HSTS), we replace $1/I_\alpha(\rho,\delta)$ by its value at the transition state, $1/I_\alpha(\rho^\#,\delta^\#)$. With these considerations, the quantum and classical effective Hamiltonians, to be used in the mixed-Q/C propagation, read

$$\begin{aligned}\hat{H}_s^{\text{eff}} &= -\frac{\hbar^2}{2\mu}\left(\frac{\partial^2}{\partial\rho^2} + \frac{1}{\rho^2}\frac{\partial^2}{\partial\delta^2}\right) + V_s^J(\rho,\delta) \\ &\quad + V_{\text{coup}}(\rho,\delta,\alpha(t)), \\ \hat{H}_b^{\text{eff}} &= \frac{p_\alpha^2}{2I_\alpha} + V_b^J(\alpha) + \langle V_{\text{coup}}(\rho,\delta,\alpha)\rangle_{\rho,\delta},\end{aligned}$$

where I_α is the constant value adopted by $1/I_\alpha(\rho,\delta)$ according to the HSMF or HSTS approximations.

3. Numerical Details

In full-QM computations, the eigenfunctions $|u_j\rangle$ were obtained by diagonalizing the representation

of $\hat{F}(\beta)$ in the basis set of eigenfunctions of $\hat{H}$. This allows for a direct application of the time-evolution operator to transform $|u_j\rangle$ into $|u_j(t)\rangle$. The expansion of $|u_j\rangle$ only included eigenfunctions of $\hat{H}$ with eigenvalues smaller than the parameter E_{max}, which was set high enough to produce converged results. In turn, the eigenfunctions of $\hat{H}$ were determined by diagonalizing the representation of this operator in a particle-in-a-box DVR basis set [24]. We were careful at the time of establishing the limits of the boxes, so that the values of $|u_j(t)\rangle$ never had significant amplitude at the edges. The number of DVR points for each variable was increased until a further increase had no effect on the final results.

The procedure used to obtain the eigenfunctions of $\hat{F}_s(\beta)$ was similar to the one described in the previous paragraph for $\hat{F}(\beta)$. The only difference being that, in this case, the computation involves only two degrees of freedom. The initial values for the classical coordinate and momenta were selected at random, according to their classical Boltzmann distributions. Finally, the trajectories were propagated using an adaptation of the PICKABACK algorithm of Bornemann et al. [25],

$$
\begin{aligned}
q(t+\Delta t/2) &= q(t) + \frac{\Delta t}{2}\frac{p(t)}{\mu},\\
|u_{\mathrm{j}}(t+\Delta t/2)\rangle &= e^{-i\hat{H}_{\mathrm{s}}\Delta t/2}|u_{\mathrm{j}}(t)\rangle,\\
p(t+\Delta t) &= p(t) - \Delta t\frac{\partial V_b}{\partial q}\\
&\quad - \Delta t\langle u_{\mathrm{j}}(t+\Delta t/2)|\left(\frac{\partial V_{\mathrm{coup}}}{\partial q}\right)\\
&\quad |u_{\mathrm{j}}(t+\Delta t/2)\rangle,\\
|u_{\mathrm{j}}(t+\Delta t)\rangle &= e^{-i\hat{H}_{\mathrm{s}}\Delta t/2}e^{iV_{\mathrm{coup}}\Delta t}|u_{\mathrm{j}}(t+\Delta t/2)\rangle,\\
q(t+\Delta t) &= q(t+\Delta t/2) + \frac{\Delta t}{2}\frac{p(t+\Delta t)}{\mu}.
\end{aligned}
$$

In the above expressions, q and p refer to the classical coordinate and momentum, respectively, while the symbol $\langle\ldots\rangle$ indicates integration over the quantum variables. The calculations presented in this article were performed with the potential energy surface of Boothroyd et al. [26, 27].

4. Results and Discussion

The properties of the full-QM flux–flux correlation functions were described in the early articles of Park and Light [28] and Miller et al. [23]. More recently, Huarte-Larrañaga and Manthe [29] presented a very detailed and insightful discussion about their behaviour, as well as the characteristics of the eigenfunctions of $\hat{F}(\beta)$. Most of these descriptions also apply to mixed-Q/C computations of the reactive flux, with just a few differences that derive from the action of the environment onto the quantum subsystem. In Figure 2, we show the time integral of mixed-Q/C flux–flux correlation functions for sets of 100 trajectories run at 200 K and 1,000 K. As explained in section 2.1, the mixed-Q/C estimation of $k(T)$ is obtained by taking the average over trajectories similar to the ones shown in Figure 2.

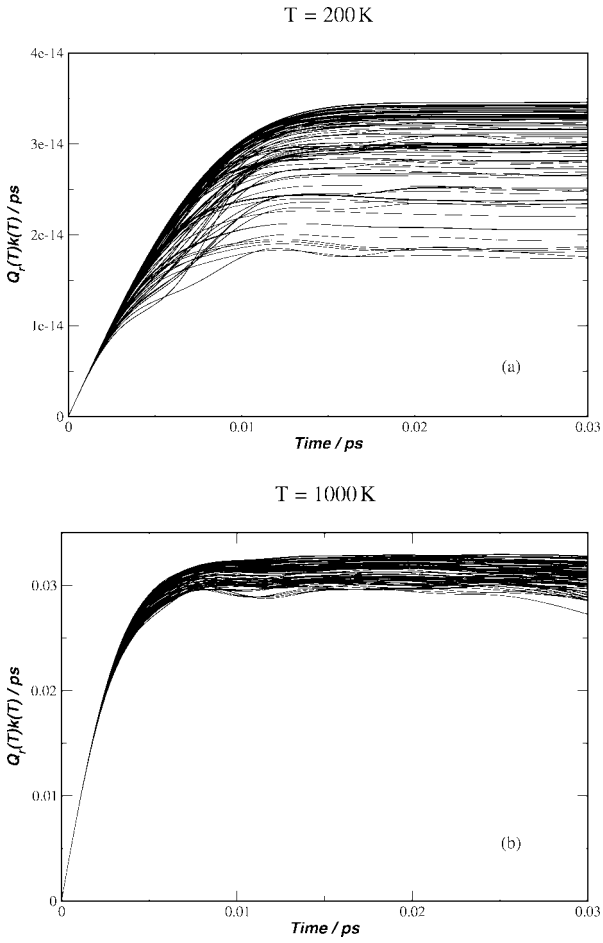

FIGURE 2. Time integrals of $C_{\mathrm{ff}}^{\mathrm{QC}}(t)$ for 100 trajectories determined using normal mode coordinates. (a) $T = 200$ K; (b) $T = 1,000$ K.

It can be noted that all the integrals reach their asymptotic value rapidly. This is typical of reactions in gas phase, which do not form long-lived complexes. Trajectories run at 1,000 K converge faster than the ones run at 200 K. This is because the higher the temperature the larger the flux, so that the initial wave packets leave the TS region more quickly. One

can also note that the dispersion between the plateau value reached by different trajectories is smaller at 1,000 K than at 200 K. Because the flux correlation function goes to zero more rapidly at higher temperatures, the quantum and classical subsystems have less time to interact. Accordingly, the behaviour of the quantum subsystem is hardly perturbed by the state of the classical one. In situations similar to this, one could resort to an even simpler but more crude approximation, in which a single trajectory for the quantum subsystem is run uncoupled from the classical bath. Then, the estimation of $C_{\mathrm{ff}}(t)$ would be evaluated by multiplying the result of that single trajectory by the partition function of the classical degrees of freedom. Such procedure could be seen as a kind of reduced dimensionality approach for the computation of the reactive flux.

For integration times larger than the ones shown in Figure 2, an unphysical behaviour in $C_{\mathrm{ff}}^{\mathrm{QC}}(t)$ is observed. Usually, the flux correlation function starts to increase and so does its time integral. This kind of misbehaviour has already been described by Park and Light [28] and Miller et al. [23] in full-QM flux–flux correlation functions. The authors attributed it to the use of a finite basis set: the time evolution of an unbound system cannot be accurately represented by a finite basis set at all times, but only within a time interval τ. The feasibility of the computation requires that the flux correlation function goes to zero for $t < \tau$, which is the case for the reaction studied in this article. It is interesting to note that, for basis sets of similar sizes, the period τ during which the calculation behaves properly is larger when using hyperspherical coordinates than when using normal modes. Also, there are differences between full-QM and mixed-Q/C computations, but in this case, the comparison cannot be done for basis sets of similar sizes. The values of $Q_r(T)k(T)$, calculated from individual Q/C trajectories, are more difficult to converge than the full-QM ones. Many of them show small oscillations at times for which the full-QM computations are already converged. However, these fluctuations are washed out when taking the average over trajectories, giving mixed-Q/C results as stable as the quantum ones.

Rate constants for $J = 0$ determined with the different Q/C approximations are plotted in Figure 3, along with the full-QM values. For completeness, the data are also presented in Table I in which we included the statistical uncertainties of the mixed-Q/C results. These uncertainties were not plotted in Figure 3, because they are almost invisible to the naked eye. It can be seen that the agreement

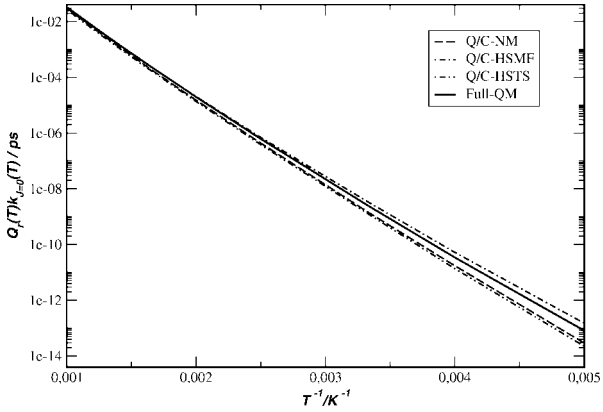

FIGURE 3. Converged values of $Q_r(T)k_{J=0}(T)$ as a function of T. Full-QM: solid line; Q/C-NM: dashed line; Q/C-HSMF: dot–dash–dot line; Q/C-HSTS: dot–dot–dash line.

between all the Q/C computations and the full-QM ones is very good above 600 K, whereas its quality starts to deteriorate below that point. At the highest temperature, the ratio between full-QM and mixed-Q/C results is 1.08 for computations performed with normal mode (NM) coordinates, 1.05 for computations that use the HSMF approximation and 1.22 for computations that use the HSTS approach. At the lowest temperature, the ratio between full-QM and mixed-Q/C results is 2.81 (NM), 3.65 (HSTS), and 0.54 (HSMF). The fact that the agreement between mixed-Q/C results and the full-QM ones is worst at the lowest temperatures revels the limitations of the mixed-Q/C schemes to accurately account for tunneling in such conditions.

It is worth noting that, while the NM and HSTS results always underestimate the rate constants, the HSMFs overestimate them for $T < 500$ K and underestimate them above that temperature. For this reason, the curve corresponding to the HSMF results crosses the full-QM one at some point between 200 K and 1,000 K. For the calculations presented in this article, the best agreement is found at $T = 600$ K where the error is less than 2%. Besides, the HSMF computations present the closest agreement with the full-QM ones over the whole temperature range. It is difficult to predict if these characteristics are general or just apply to the reaction under study. Clearly, the analysis of several reactions involving different mass combinations, as well as different topologies in their PES are needed to clarify this point. For the time being, we can only say that the HSMF scheme appears as the most promising one among those analyzed in this work.

TABLE I

Converged values of $Q_r(T)k(T)$/ps for J=0.

T (K)	Full-QM	Q/C-NM	Q/C-HSTS	Q/C-HSMF
200	$8.19e-14$	$2.92(0.05)e-14$	$2.25(0.02)e-14$	$1.51(0.02)e-13$
250	$3.45e-11$	$1.74(0.03)e-11$	$1.37(0.02)e-11$	$5.26(0.03)e-11$
300	$2.43e-09$	$1.42(0.03)e-09$	$1.23(0.02)e-09$	$3.30(0.03)e-09$
400	$6.20e-07$	$4.37(0.03)e-07$	$3.86(0.04)e-07$	$6.70(0.05)e-07$
500	$1.98e-05$	$1.52(0.01)e-05$	$1.36(0.01)e-05$	$2.05(0.02)e-05$
600	$2.16e-04$	$1.71(0.02)e-04$	$1.56(0.02)e-04$	$2.12(0.01)e-04$
700	$1.24e-03$	$1.03(0.03)e-03$	$9.35(0.09)e-04$	$1.19(0.01)e-03$
800	$4.78e-03$	$4.14(0.02)e-03$	$3.70(0.03)e-03$	$4.52(0.03)e-03$
900	$1.41e-02$	$1.25(0.01)e-02$	$1.11(0.02)e-02$	$1.32(0.02)e-02$
1000	$3.33e-02$	$3.07(0.01)e-02$	$2.73(0.02)e-02$	$3.16(0.02)e-02$

The statistical uncertainty of the Q/C results is given within parenthesis.

Full-QM and mixed-Q/C HSMF rate constants, calculated by summing up the contribution of the different values of J, are plotted in Figure 4. Because we considered a planar system, these rates were calculated as

$$k(T) = k_{J=0}(T) + 2\sum_{J=1}^{N} k_J(T). \tag{18}$$

The figure illustrates that, in accordance with the results of $J = 0$ computations, the agreement between full-QM and mixed-Q/C results is pretty good. The Q/C rates overestimate the full-QM ones at low temperatures and slightly underestimate them at high temperatures. Finally, we should mention that total rate constants were also calculated from $J = 0$ mixed-Q/C computations invoking the J- shifting approximation [30],

$$k(T) \cong Q^{\#}_{\mathrm{rot}}(T)k_{J=0}(T), \tag{19}$$

where $Q^{\#}_{\mathrm{rot}}(T)$ is the rotational partition function calculated at the TS. We found that the mixed-Q/C results obtained from Eq. (19) are very close to those calculated with Eq. (18). At $T = 300$, 600, and 1000 K, the results of the J-shifting approximation underestimate those obtained with Eq. (18) by 4%, 5%, and 6%, respectively. Thus, the error introduced by the use of Eq. (19) is of the same order (or even lower) than the one introduced by the mixed-Q/C approach. Assuming that these observations will also hold for computations in three dimensions, one is lead to conclude that mixed-Q/C evaluations of $k(T)$ could be done with the much cheaper J-shifting approximation without a significant loss of accuracy.

The mixed-Q/C computations described so far have two degrees of freedom in the quantum subsystem and just one in the classical subsystem. We also tested a model with a single quantum degree of freedom. Basically, we worked with the Hamiltonian in normal modes for $J = 0$ and considered quantally the mode associated with the imaginary frequency. With such a model, we were unable to get converged results because the flux–flux correlation function presents large oscillations that do not go to zero within a reasonable time. This failure can be explained by noting that, in a region nearby the TS, slices of the PES along the quantum coordinate are symmetrical double wells. So, the situation is reminiscent to the one found in condensed-phase reactions. In such conditions, $k(T)$ can only be defined

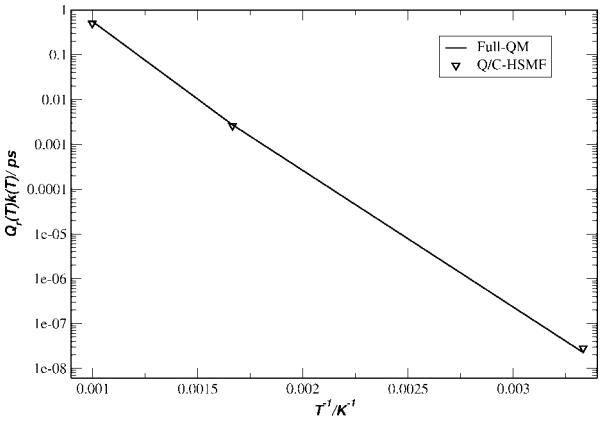

FIGURE 4. Converged values of $Q_r(T)k(T)$ as a function of T. Full-QM: solid line; Q/C-HSMF:white triangles.

if the interaction with the bath is strong enough to break the symmetry of the potential and keep the wave packet trapped in one of the wells for long enough [31]. For the title reaction, this condition is not fulfilled and the flux correlation function oscillates endlessly. Probably, other definitions of a single quantum coordinate could give better mixed-Q/C schemes. However, instead of pursuing the search of such coordinate, we decided to follow an alternative way that consisted on defining quantum subsystems with two degrees of freedom. These two degrees of freedom ($\{q_1, q_2\}$ or $\{\rho, \delta\}$) describe, altogether, the bonds being broken and formed, and guarantee that the motion of the wave packet is unbound so that the flux–flux correlation function converges within a reasonable propagation time. Also, we believe that the use of two quantum degrees of freedom, instead of one, is important to obtain a better description of tunnelling. This is because the symmetric vibration at the TS modulates the distance between the donor and the acceptor of the atom being transferred, and this distance has a large influence on the tunnel probability.

5. Concluding Remarks

We have presented mixed-Q/C schemes to estimate the flux correlation function of three-atom reactions. The accuracy of these schemes was tested by comparing their results against those obtained in full-quantum computations. The system under analysis was a planar version of the $H+H_2 \rightarrow H_2+H$ reaction. We found that, for temperatures above 500 K, all the algorithms produce results in close agreement with the full-quantum ones. Below that temperature, the agreement starts to deteriorate. The best results were obtained with the HSMF scheme, which gives a quantum treatment to the hyperspherical coordinates $\{\rho, \delta\}$ and treats classically the angle that describes the bending motion at the TS. Another approximation invoked by this scheme is that it replaces the factor $1/I_\alpha(\rho, \delta)$, appearing in Eq. (13), by the average of this function over the lowest eigenfunction of $\hat{F}_s(\beta)$.

Mixed-Q/C schemes such as the ones analyzed in this article present several characteristics that are appealing in any approximate method aimed to calculate $k(T)$. These are their conceptual simplicity, low computational cost, and ability to take into account tunnelling and recrossings without needing *ad hoc* corrections. Because of these characteristics and of the good results determined so far, we believe these are very promising approaches. However, we should note that further tests still need to be done on more challenging systems, in order to thoroughly evaluate their capabilities. In particular, it should be important to evaluate the quality of mixed-Q/C schemes in reactions with asymmetric potential energy surfaces. Previous implementations, based on reactive scattering theory, found difficulties in those cases [13]. It would also be valuable to analyze the performance of the approach when treating polyatomic reactions that involve fragments with several internal degrees of freedom. To this end, reactions of the type $X+CH_4 \rightarrow XH+CH_3$ with X=H, O(^{3}P) are obvious candidates because of the existence of accurate full-quantum results [32], which could be used as benchmarks. In that regard, we should note that the mixed-Q/C schemes presented in this article could be easily extended to treat larger systems. This also constitutes a valuable characteristic of the proposed approach.

Appendix

To obtain the equations of motion corresponding to the Hamiltonian of Eq. (12), we followed the procedure described by Gerber et al. [22]. With that aim, it is convenient to rewrite the Hamiltonian as,

$$\hat{H} = \hat{K}_s(\rho, \delta) + f(\rho, \delta)\hat{K}_b(\alpha) + V^J(\rho, \delta, \alpha), \qquad (20)$$

where the kinetic energy operator $\hat{K}_s$ acts on variables ρ and δ, and $\hat{K}_b$ acts on variable α. However, because of the presence of the function $f(\rho, \delta) = I_\alpha(\rho, \delta)^{-1}$, the second term depends parametrically on ρ and δ. For this Hamiltonian, we look for solutions of the time-dependent Schrödinger equation in the form of a Hartree product,

$$\psi(\rho, \delta, t) = \phi_s(\rho, \delta, t)\phi_b(\alpha, t), \qquad (21)$$

or in a more simplified way $|\psi\rangle = |\phi_s\rangle|\phi_b\rangle$. By invoking the Dirac–Frenkel–McLachlan variational principle [33], this trial function leads to the following equations of motion

$$\left(\langle\phi'_s \mid f \mid \phi'_s\rangle\hat{K}_b + \langle\phi'_s \mid V^J \mid \phi'_s\rangle\right) \mid \phi'_b\rangle = i\hbar\frac{\partial \mid \phi'_b\rangle}{\partial t},$$
$$(\hat{K}_s + \langle\phi'_b \mid \hat{K}_b \mid \phi'_b\rangle f + \langle\phi'_b \mid V^J \mid \phi'_b\rangle) \mid \phi'_s\rangle = i\hbar\frac{\partial \mid \phi'_s\rangle}{\partial t}$$

where $|\phi'_s\rangle$ and $|\phi'_b\rangle$ are related to $|\phi_s\rangle$ and $|\phi_b\rangle$ by a phase factor of no importance $|\phi'_s\rangle = \exp[i\sigma_s(t)]|\phi_s\rangle$; $|\phi'_b\rangle = \exp[i\sigma_b(t)]|\phi_b\rangle$ [22].

Then, we consider that the wave function for the bath variable has the form

$$\phi'_{\mathrm{b}} = a(\alpha, t) \exp\left(\frac{iS(\alpha, t)}{\hbar}\right), \tag{22}$$

where $|a(\alpha, t)|^2$ is an approximate Dirac δ function at position $\alpha(t)$. Introducing this function into the equations of motion presented above and taking the classical limit ($\hbar \to 0$), we arrive at the following set of equations,

$$\frac{1}{2}\langle\phi'_{\mathrm{s}} \mid f \mid \phi'_{\mathrm{s}}\rangle \left(\frac{\partial S}{\partial \alpha}\right)^2 + \langle\phi'_{\mathrm{s}} \mid V^J \mid \phi'_{\mathrm{s}}\rangle = -\frac{\partial S}{\partial t},$$
$$\left(\hat{K}_{\mathrm{s}} + \frac{1}{2}\left(\frac{\partial S}{\partial \alpha}\right)^2 f + V^J(\alpha(t))\right) \mid \phi'_{\mathrm{s}}\rangle = i\hbar \frac{\partial \mid \phi'_{\mathrm{s}}\rangle}{\partial t}.$$

The first of these expressions is a Hamilton–Jacobi equation for the generating function $S(\alpha, t)$, whose associated momentum is

$$p_\alpha = \frac{\partial S}{\partial \alpha}. \tag{23}$$

It leads to the following equations of motion for the classical variable α

$$\dot{p_\alpha} = -\frac{\partial H_b^{\mathrm{eff}}}{\partial \alpha},$$
$$\dot{\alpha} = \frac{\partial H_b^{\mathrm{eff}}}{\partial p_\alpha}$$

with,

$$H_{\mathrm{b}}^{\mathrm{eff}} = \frac{1}{2}\langle\phi'_s \mid f \mid \phi'_{\mathrm{s}}\rangle p_\alpha^2 + \langle\phi'_{\mathrm{s}} \mid V^J \mid \phi'_{\mathrm{s}}\rangle. \tag{24}$$

On the other hand, the propagation equation for the quantum subsystem can be written as

$$\hat{H}_{\mathrm{s}}^{\mathrm{eff}} \mid \phi'_{\mathrm{s}}\rangle = i\hbar \frac{\partial \mid \phi'_{\mathrm{s}}\rangle}{\partial t}, \tag{25}$$

with

$$\hat{H}_{\mathrm{s}}^{\mathrm{eff}} = \hat{K}_{\mathrm{s}} + \frac{1}{2} p_\alpha^2(t) f + V^J(\alpha(t)). \tag{26}$$

The effective classical Hamiltonian of Eq. (24) differs from the one corresponding to standard mixed-Q/C schemes by the factor $\langle\phi'_{\mathrm{s}} \mid f \mid \phi'_{\mathrm{s}}\rangle$, which multiplies to the classical momentum. This factor depends on time because ϕ'_{s} is a time dependent function. Accordingly, it has to be updated at every step of the numerical propagation. The effective quantum Hamiltonian of Eq. (26) also differs from the one obtained in standard mixed-Q/C schemes. In this case, the difference appears because of the presence of the term $\frac{1}{2}p_\alpha^2(t)f$, which is absent in the standard scheme. This term plays the role of a time-dependent potential and can be added to V^J at the moment of performing the numerical propagation.

Trajectories run with the effective Hamiltonians of Eqs. (24) and (26) take a little longer than the ones computed with the HSMF approach. Besides, the conservation of energy is not as good as in the standard scheme. This could be due to the fact that the PICKABACK algorithm, used to propagate the mixed-Q/C equations of motion, has been designed to optimize the energy conservation when the propagation equations have the standard form. We also noted that the statistical uncertainty of the results is somewhat larger when we used the equations of motion derived in this appendix. Nevertheless, the averaged values determined by the two schemes agree with each other within their statistical uncertainties. Thus, there seems to be no advantages in using the more complex propagation scheme derived here. Accordingly, we consider advisable the use of schemes such as HSMF that conserve the form of the more familiar and well-tested standard equations of motion.

ACKNOWLEDGMENTS

The authors thank CONICET for postdoctoral fellowship awarded to E.C.

References

1. Palma, J. J Chem Phys 2009, 130, 124119.
2. McRae, R. P.; Schenter, G. K.; Garrett, B. C.; Haynes, G. R.; Voth, G. A.; Schatz, G. C. J Chem Phys 1992, 97, 7392.
3. Neuhauser, D.; Judson, R. S. Chem Phys Lett 1991, 179, 385.
4. Adhikari, S.; Billing, G. D. Chem Phys 1998, 238, 69.
5. Markovic, N.; Billing, G. D. Chem Phys 1993, 173, 385.
6. Billing, G. D.; Markovic, N. Chem Phys 1996, 209, 377.
7. Markovc, N.; Billing, G. D. Chem Phys 1997, 224, 53.
8. Balakrishnan, N.; Billing, G. D. Chem Phys 1994, 189, 499.
9. Balakrishnan, N.; Billing, G. D. J Chem Phys 1994, 101, 2785.
10. Wang, L.; Clary, D. C. Chem Phys Lett 1996, 262, 284.
11. Wang, L.; Clary, D. C. J Chem Phys 1996, 104, 5663.
12. Wang, L.; McCoy, A. B. Phys Chem Chem Phys 1999, 1, 1227.
13. Wang, L.; Meurer, W. J.; McCoy, A. B. J Chem Phys 2000, 113, 10605.
14. Wang, L.; McCoy, A. B. J Chem Phys 2003, 119, 1996.

15. Wang, L. J Chem Phys 1998, 108, 7538.
16. Wang, L. Chem Phys Lett 2004, 383, 62.
17. Wang, L. Phys Chem Chem Phys 2000, 2, 2883.
18. Cui, Q.; He, X.; Wang, M. L.; Zhang, J. Z. H. J Chem Phys 2003, 119, 9455.
19. Wang, M.; Zhang, J. Z. H. J Chem Phys 2003, 119, 11152.
20. Wang, H.; Sun, X.; Miller, W. H. J Chem Phys 1998, 108, 9726.
21. Truong, T. N.; McCammon, J. A.; Kouri, D. J.; Hoffman, D. K. J Chem Phys 1992, 96, 8136.
22. Gerber, R. B.; Buch, V.; Ratner, M. A. J Chem Phys 1982, 77, 3022.
23. Light, J. C.; Hamilton, I. P.; Lill, J. V. J Chem Phys 1985, 82, 1400.
24. Bornemann, F. A.; Nettesheim, P.; Schutte, C. J Chem Phys 1996, 105, 1074.
25. Boothroyd, A. I.; Keogh, W. J.; Martin, P. G.; Peterson, M. R. J Chem Phys 1991, 95, 4343.
26. Boothroyd, A. I.; Keogh, W. J.; Martin, P. G.; Peterson, M. R. J Chem Phys 1996, 104, 7139.
27. Park, T. J.; Light, J. C. J Chem Phys 1989, 91, 974.
28. Miller, W. H.; Schwartz, S. D.; Tromp, J. W. J Chem Phys 1983, 79, 4889.
29. Huarte-Larrañaga, F.; Manthe, U. Multidimensional Quantum Dynamics: MCTDH Theory and Applications; Wiley: Wiley-VCH Verlag GmbH & Co. KGaA, 2009.
30. Bowman, J. M. J Phys Chem 1991, 95, 4960.
31. Chandler, D. J Chem Phys 1978, 68, 2959.
32. Wu, T.; Werner, H.; Manthe, U. Science 2004, 306, 2227.
33. McLachlan, A. D. Mol Phy 1964, 8, 39.